Applied Catalysis B: Environmental 306 (2022) 121108

Contents lists available at ScienceDirect

Applied Catalysis B: Environmental

journal homepage: www.elsevier.com/locate/apcatb

Effect of redox promoters (CeO_x and CuO_x) and surface sulfates on the selective catalytic reduction (SCR) of NO with NH_3 by supported V_2O_5-WO_3/TiO_2 catalysts

Mingyu Guo [a,b,1], Bar Mosevitzky Lis [a,1], Michael E. Ford [a], Israel E. Wachs [a,*]

[a] Operando Molecular Spectroscopy & Catalysis Laboratory, Department of Chemical and Biomolecular Engineering, Lehigh University, Bethlehem, PA 18015, USA
[b] Tianjin Key Laboratory of Indoor Air Environmental Quality Control, School of Environmental Science and Engineering, Tianjin University, Tianjin 300350, China

ARTICLE INFO

Keywords:
SCR
Catalysts
Supported V_2O_5-WO_3/TiO_2
Promoters
Redox
Ceria
Copper
Spectroscopy
Raman
Infrared
Temperature-programmed surface reaction (TPSR)

ABSTRACT

A series of TiO_2-supported MO_x catalysts (M=V, W, Ce, Cu and S) were investigated for their SCR activity. *In situ* Raman spectroscopy indicated that the supported MO_x phases were completely dispersed as surface sites on the TiO_2 support. *In situ* IR revealed that surface VO_x, WO_x and SO_x sites anchored at both CeO_x/CuO_x and TiO_2 sites. The number of surface Lewis acid sites decreased with the addition of basic (CeO_x/CuO_x) and acidic (VO_x/WO_x) sites in all catalysts, and acidic SO_x in the unpromoted and Ce-promoted catalysts. The surface VO_x, WO_x and SO_x sites introduced surface Brønsted acid sites. The redox promoters increased the NO conversion, but SO_x impregnation inhibited their effect due to acid (SO_x)-base (CeO_x/CuO_x) interactions. The SCR reaction was shown to efficiently proceed via either surface NH_3* or NH_4^+* species, resolving the long-standing dispute on the involvement of these species in the SCR reaction.

1. Introduction

Selective catalytic reduction (SCR) is widely used to mitigate NO_x emissions [1,2] by utilizing reducing gasses coupled with heterogeneous catalysts [3,4]. Supported V_2O_5-WO_3/TiO_2 is the most prolific SCR catalyst owing partially to its lower cost compared to zeolite-based catalysts [5,6]. Its vanadia component acts as the active redox site while the tungsta promotes the VO_x redox activity and generates surface Brønsted acid sites [7,8]. The operational temperature range of supported V_2O_5-WO_3/TiO_2 is ~300–400 °C [9,10], with VO_x sites generating the greenhouse gas N_2O from NH_3 over-oxidation at high temperatures [10], though to a lower extent when H_2O is present in the treated gas mixture [11]. Recently, the catalyst has garnered attention for its pollutant abatement applicability in compression-ignition engine vehicles [12–17]. However, emissions under cold start conditions remain high due to the catalyst's limited activity at low temperatures [18–21]. Thus, the supported V_2O_5-WO_3/TiO_2 SCR catalyst is incapable of meeting current need for high activity at low temperatures.

Previous studies have demonstrated that the SCR performance of supported V_2O_5-WO_3/TiO_2 at low temperatures can be enhanced by the addition of redox promoters [22–24]. Among them, cerium and copper oxides have received attention because of their ability to easily cycle between Ce^{4+}/Ce^{3+} and Cu^{2+}/Cu^{+} oxidation states[25,26]. These capabilities improve the catalysts' redox performance and, thereby, enhance catalytic oxidation activity [27,28]. Several CeO_x promoted catalysts have been shown to be SCR active (e.g., $CeWO_x$ [23,29], $VCeO_x$ [30,31] and $MnCeO_x$ [32,33]). Vuong et al. investigated a mixed CeO_2-TiO_2 support system synthesized by co-precipitation and demonstrated improved redox performance due to highly dispersed VO_x sites anchored at both CeO_2 (V-O-Ce) and Ti (V-O-Ti) sites [14]. Michalow-Mauke et al. proposed that the presence of CeO_2 in flame pyrolyzed $WCeTiO_x$ generated bridging Ce-O-W and Ce-O-Ti bonds that were critical for SCR performance [25]. Ma et al. reported that a Ce-modified V_2O_5-WO_3/TiO_2 catalyst, where the W-Ti-Ce mixed oxide support was synthesized by a citric acid-aided sol-gel method and VO_x impregnated with an aqueous NH_4VO_3 solution, was active for SCR at

* Corresponding author.
E-mail address: iew0@lehigh.edu (I.E. Wachs).
[1] Mingyu Guo and Bar Mosevitzky Lis contributed equally to this work.

https://doi.org/10.1016/j.apcatb.2022.121108
Received 1 February 2021; Received in revised form 11 January 2022; Accepted 14 January 2022
Available online 18 January 2022
0926-3373/© 2022 Elsevier B.V. All rights reserved.

low temperatures [34]. Studies on supported CuO/Al_2O_3 showed that CuO possesses good redox properties [35,36]. A CuO promoted supported V_2O_5-WO_3/TiO_2 catalyst demonstrated enhanced redox properties in Hg^0 oxidation and SCR [37,38]. Despite such reports on the enhancing effects of CeO_x and CuO_x on SCR catalysts, few fundamental studies have been published of these redox promoted V_2O_5-WO_3/TiO_2 SCR catalysts.

In industrial applications, SO_2 is also present in flue gas emissions and results in the formation of surface sulfates, ammonium sulfates and metallic sulfates that affect SCR activity. Ammonium sulfates, generated by oxidation of SO_2 into SO_3 and the subsequent reaction of SO_3 with NH_3 and water [39], promote the formation of haze and acid rain [40]. Although the surface sulfates can improve SCR performance by contributing to surface acidity [33,34,41,42], the deposition of ammonium sulfates on the catalysts and downstream in the process can lead to detrimental effects [39,43].

In this study, the CeO_x and CuO_x redox promoted and sulfate-free and sulfated supported V_2O_5-WO_3/TiO_2 catalysts were synthesized by the incipient-wetness impregnation method. The interactions of CeO_x, CuO_x and SO_x with the TiO_2 support and dispersed VO_x and WO_x, and their molecular structures were investigated with *in situ* Raman and Infrared (IR) spectroscopies, while the surface acidity of the catalysts was chemically probed with adsorbed ammonia that was monitored with *in situ* IR. The effects of the surface CeO_x and CuO_x redox promoters and sulfates upon the SCR performance and selectivity of the supported V_2O_5-WO_3/TiO_2 catalysts were examined with temperature-programmed surface reaction (TPSR) spectroscopy. These results enabled the establishment of structure-activity relationships for the redox promoted, sulfate-free and sulfated, supported V_2O_5-WO_3/TiO_2 catalysts.

2. Experimental

2.1. Catalyst preparation

The incipient-wetness impregnation method was utilized to synthesize the TiO_2-supported catalysts. Both isolated and oligomeric surface oxide sites can be present under monolayer coverage, while crystalline nanoparticles (NPs) develop when exceeding monolayer coverage [44,45]. Previous studies showed that the dispersion capacities of CeO_2 and CuO are both ~7 cations/nm^2 on TiO_2 supports [46,47]. Initially, 80% monolayer coverages of CeO_2 (7.9 wt%, precursor: $Ce(NO_3)_3{\cdot}6H_2O$, 99.99%, Alfa Aesar) and CuO (3.8 wt%, precursor: $Cu(NO_3)_2{\cdot}2.5H_2O$, 99.99%, Alfa Aesar) were separately impregnated on TiO_2 (Evonik P-25; ~55 m^2/g; ~80% anatase and ~20% rutile). An example of the monolayer calculation for CeO_2 is shown in Eq. S1 [48]. The precursors were added to the TiO_2 in a drop-wise manner under constant stirring. After 45 min of mixing, the samples were dried overnight at room temperature and then dehydrated under synthetic air (Airgas, 100 cc min^{-1}) at 120 °C for 2 hr and finally calcined at 450 °C (heating at a rate of 1 °C min^{-1}) for 4 hr. Subsequently, VO_x (1 wt%, precursor: NH_4VO_3, 99.0%, Alfa Aesar) was impregnated onto the redox promoted TiO_2, which was dried and calcined at the same conditions mentioned above. This was followed by the impregnation of WO_x (5 wt%, precursor: $(NH_4)_6H_2W_{12}O_{40}{\cdot}XH_2O$, 99.9%, Strem Chemicals), dehydration and calcination. Lastly, SO_x (1.5 wt%, precursor: $(NH_4)_2SO_4$, 99.0%, Sigma-Aldrich) was impregnated onto the catalysts which were similarly dried and calcined.

2.2. Catalyst characterization

2.2.1. BET specific surface area measurement

The surface areas of the catalysts were measured by N_2 adsorption-desorption (BET) using 100 mg samples with an ASAP 2020 HD88 (Micromeritics, USA). Prior to the measurement, the catalysts were dehydrated at 300 °C for 5 h to remove moisture and any adsorbed impurities from their surface.

2.2.2. In situ Raman spectroscopy

The molecular structures of the supported MO_x sites were analyzed with *in situ* Raman spectroscopy. The Raman measurements were performed with visible wavelength (532 nm) laser excitation on a single stage Horiba-Jobin Yvon Lab Ram-HR Raman spectrometer with a confocal microscope (Olympus BX-30) and a notch filter (Kaiser Super Notch). The beam was generated by a Nd-YAG double diode pumped laser (Coherent Compass 315 M-150, output power of 150 mW with power at the sample of 10 mW). The scattered photons were directed into a single monochromator and focused unto a UV-sensitive liquid N_2 cooled charge coupled device detector (Horiba-Jobin Yvon CCD-3000 V) with a spectral resolution of ~1 cm^{-1} at the applied parameters. Powder catalysts were loaded into a reaction cell (Harrick Scientific HVC-DRP4) and connected to a gas flow control system. A Harrick ATC Temperature Controller unit controlled the catalyst temperature. Catalyst dehydration was performed by flowing 10% O_2/Ar (Airgas, 30 cc min^{-1}) at 400 °C for 1 hr prior to acquiring the *in situ* Raman spectra measurements at 400 °C. The data used to plot the relevant Raman figures presented herein is provided in the SI.

2.2.3. In situ infrared spectroscopy

In situ IR spectra were collected with a Fourier-transform infrared (FTIR) spectrometer (Thermo NICOLET 8700) equipped with a high sensitivity mercury-cadmium-telluride (MCT-A) detector and a Harrick Praying Mantis Attachment (Model DRA-2) for diffuse reflectance spectroscopy. Powder catalysts were loaded into a Harrick Scientific reaction cell (HVC-DRP4) which was connected to a gas flow control system. The reaction cell temperature was controlled with a Harrick ATC Temperature Controller unit. In each experiment, the catalyst was heated to 400 °C (heating at a rate of 10 °C min^{-1}) and held for 1 hr in 10% O_2/Ar (30 cc min^{-1}), after which the *in situ* IR spectra were collected for the dehydrated catalyst. Ammonia temperature programmed desorption (TPD) was used to measure the catalysts' acidity and number of acid sites. To achieve this, each catalyst was cooled from 400 °C to 110/200/250 °C, held at that temperature under 2000 ppm NH_3/He (PRAXAIR, 35 cc min^{-1}) and left to soak for 30 min, followed by flowing He (PRAXAIR, 30 cc min^{-1}) for another 30 min. Finally, the catalyst was heated to 500 °C (heating at a rate of 10 °C min^{-1}) under He (30 cc min^{-1}). The IR spectra were collected at 1 min intervals. All the reported *in situ* IR spectra intensities were normalized with respect to the TiO_2 support's IR band at ~920 cm^{-1} as an internal standard. The IR peaks at ~1230 cm^{-1} and ~1450 cm^{-1} were integrated to quantify the surface NH_3 * and NH_4^+* species on Lewis and Brønsted acid sites, respectively [5,9]. The data used to plot the relevant IR figures presented herein is provided in the SI.

2.2.4. Temperature-programmed surface reaction (TPSR) spectroscopy

An Altamira AMI-200 system equipped with a Dycor Dymaxion DME200MS online quadrupole mass spectrometer (MS) was used to measure the SCR activity. A fixed-bed reactor consisting of a U-type quartz tube loaded with 30 mg of catalyst fixed in place by quartz wool. The catalysts were initially heated to 400 °C (heating at a rate of 10 °C min^{-1}) under 5% O_2/He (50 cc min^{-1}), holding for 1 hr at 400 °C, and then cooled to 100 °C. After cooling, a 2000 ppm NH_3/He (35 cc min^{-1}), 2000 ppm NO/He (35 cc min^{-1}) and 5% O_2/He (5 cc min^{-1}) mixture was introduced into the reactor and the system was heated to 500 °C (10 °C min^{-1} heating rate). A lower than standard O_2 concentration was used herein to mitigate damage to the mass spectrometer, possibly highlighting the effect of the redox promoters and resulting in a modest shift of the NO conversion curve to higher temperatures (Fig. S1) than previously demonstrated for the V_2O_5-WO_3/TiO_2 catalyst system [49]. In the NO-free TPSR experiments, a mixture of 2000 ppm NH_3/He (35 cc min^{-1}), He (35 cc min^{-1}) and 5% O_2/He (5 cc min^{-1}) was used instead. The outlet gas compositions were analyzed by the online MS to follow

the catalytic activity as a function of temperature. The following mass to charge (m/z) ratios were used for species identification: NO ($m/z = 30$), N_2O ($m/z = 44$), NH_3 ($m/z = 17$), N_2 ($m/z = 28$), H_2O ($m/z = 18$), and NO_2 ($m/z = 46$). No NO_2 was formed in any of the TPSR experiments described in this work. The data used to plot the relevant TPSR figures presented herein is provided in the SI.

3. Results and discussion

3.1. Anchoring surface sites of supported CeO_x/TiO_2 and CuO_x/TiO_2 catalysts

It is well established that surface metal oxides anchor at surface hydroxyls of oxide supports [50–52]. The *in situ* IR difference spectra of the dehydrated TiO_2 and redox promoted TiO_2 before and after VO_x impregnation in the surface hydroxyl region (3450–3850 cm^{-1}) are presented in Fig. 1. The original spectra from which the difference spectra were calculated are provided in Fig. S2. The TiO_2 support possesses basic terminal Ti-(OH) (3710 cm^{-1}) and more acidic bridging Ti-(OH)-Ti (3674, 3661 and 3630 cm^{-1}) surface hydroxyls [5,53]. Impregnation of 1%V_2O_5 onto the TiO_2 support titrates nearly all of the Ti-(OH), some of the Ti-(OH)-Ti (3674 cm^{-1}), and generates new surface hydroxyls assigned to Ti-(OH)-V (3640 cm^{-1}) as shown in Fig. 1 [54–56]. The CeO_x promoter anchors at the more acidic Ti-(OH)-Ti surface hydroxyls (3661 and 3630 cm^{-1}) and generates more basic Ce-(OH) (3710 cm^{-1}) surface hydroxyls (Fig. 1a) [57–59]. Generation of Ce-(OH)-Ce and Ce-(OH)-Ti (3674, 3660 and 3630 cm^{-1}) surface hydroxyls due to anchoring of CeO_x at Ti-hydroxyls is likely, but cannot be ascertained due to overlap in the Ti- and Ce-hydroxyl vibrations. Further impregnation of 1%V_2O_5 titrates all the Ti-(OH) and Ce-(OH) and some of the M-(OH)-M (M=Ce or Ti) surface hydroxyls. The supported CuO_x promoter anchors at both Ti-(OH)-Ti (3661 cm^{-1}) and Ti-(OH) surface hydroxyls (3710 cm^{-1}) and appears to generate Cu-(OH)-Cu (3565 cm^{-1}) surface hydroxyls (Fig. 1b) [60–62]. Impregnating 1%V_2O_5 onto the CuO/TiO_2 support titrates most of the Cu-(OH)-Cu (3565 cm^{-1}) and some of the Ti-(OH)-Ti (3674 and 3630 cm^{-1}) surface hydroxyls as shown in Fig. 1. This behavior indicates that the impregnated VO_x surface sites anchor preferentially on the redox surface hydroxyls, forming unique M-O-V ligands in the process.

Impregnation of 5% WO_3 onto the supported V_2O_5/TiO_2 catalyst titrates additional Ti-(OH)-V and Ti-(OH)-Ti (3661 cm^{-1}) surface hydroxyls as shown in Fig. 2a. The original spectra from which the difference spectra were calculated are shown in Fig. S3. For the supported $WO_3/V_2O_5/CeO_2/TiO_2$ catalyst, essentially all the surface hydroxyls are consumed. For the supported $WO_3/V_2O_5/CuO/TiO_2$ catalyst, the Ti-(OH)-Ti (3674/3661 cm^{-1}) and Cu-(OH)-Cu (3565 cm^{-1}) surface hydroxyls are consumed leaving only a minor amount of more acidic ($\leq$ 3645 cm^{-1}) surface hydroxyls. Although a considerable amount of residual surface hydroxyls remained for the unpromoted catalyst (Fig. S3), only low levels of surface hydroxyls were present for the CuO_x promoted catalyst (Fig. S3b) and virtually no surface hydroxyls were present for the CeO_x promoted catalyst (Fig. S3a), possibly due to their more basic character compared to TiO_2 [63,64]. This relative lack of surface hydroxyl signals in the CeO_x promoted catalyst's spectrum compared to the unpromoted catalyst reflects the Ce-induced improved dispersion of the surface VO_x and WO_x sites within the monolayer. Overall, these results demonstrate that redox promotion of supported $WO_3/V_2O_5/TiO_2$ catalysts leads to higher consumption of Ti, Ce and Cu surface hydroxyls, with both VO_x and WO_x sites preferentially titrating the more basic surface hydroxyls on all supports. While only a minor portion of the VO_x and WO_x sites anchored to the redox surface hydroxyls in the Cu promoted catalyst, the redox surface hydroxyls in the Ce promoted catalyst made up the bulk of the VO_x and WO_x anchoring sites. The relatively similar BET surface area of the promoted and unpromoted catalysts suggests that the redox promotion does not significantly alter the surface morphology (Table S1).

The *in situ* IR spectra of the surface hydroxyl region for the dehydrated SO_x impregnated catalysts are presented in Fig. 2b. The original spectra from which the difference spectra were calculated are shown in Fig. S4. Impregnation of the supported $WO_3/V_2O_5/TiO_2$ catalyst with 1.5% SO_x consumes most of the remaining Ti surface hydroxyls. Anchoring of SO_4 on bare TiO_2 support is known to preferentially consume the basic terminal surface hydroxyls due to acid-base interactions [65]. Sulfation of the CeO_x promoted supported $WO_3/V_2O_5/CeO_2/TiO_2$ catalyst exposes Ce-(OH)-Ce and possibly Ce_3-(OH) surface

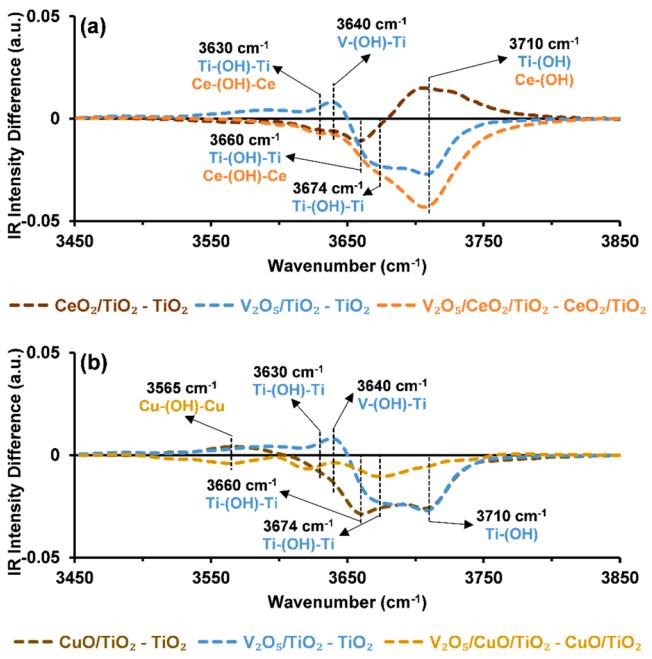

Fig. 1. *In situ* IR difference spectra of the hydroxyl region from dehydrated TiO_2 supported VO_x-free and VO_x impregnated (a) CeO_x promoted and (b) CuO_x promoted catalysts (spectra collected at 400 °C under 10% O_2/Ar flow).

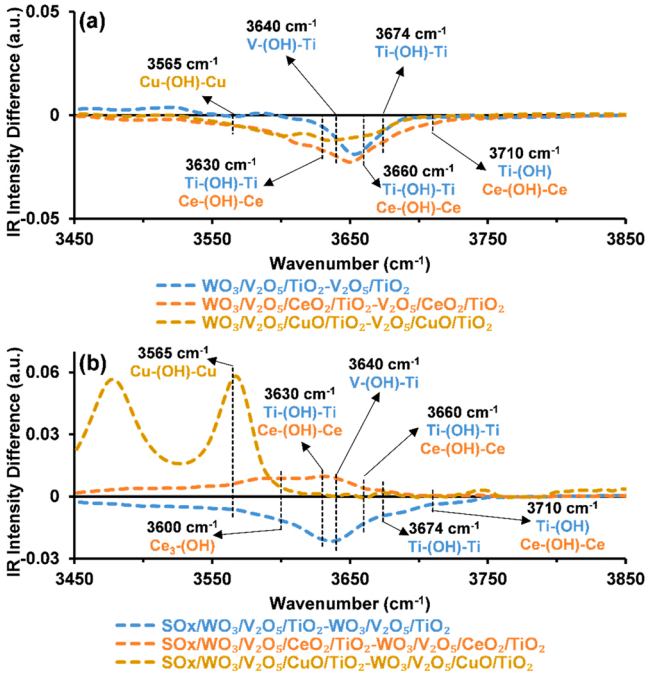

Fig. 2. *In situ* IR spectra of the hydroxyl region of the dehydrated supported redox promoted (a) WO_x-impregnated and (b) sulfated catalysts (spectra collected at 400 °C in flowing 10% O_2/Ar).

hydroxyls (3630 and 3600 cm^{-1}, respectively) [66,67]. New vibrations at 3570 cm^{-1} and 3484 cm^{-1} were detected after SO_x impregnation onto the CuO_x promoted supported $WO_3/V_2O_5/CuO/TiO_2$ catalyst, possibly corresponding to exposed Cu-(OH)-Cu surface hydroxyls (3565 cm^{-1}). The sulfated unpromoted and CeO_x promoted catalysts exhibited similar surface hydroxyl distributions (Fig. S4a), while the sulfated CuO_x promoted catalyst had significant surface concentrations of highly acidic Cu surface hydroxyls exposed by sulfation (Fig. S4a). This suggests that the vanadia and tungsta species previously bound to the redox promoters were displaced by the more acidic SO_x species, thereby exposing previously covered hydroxyls. This behavior is further evidenced by the more significant changes in BET surface area due to sulfation in the redox promoted catalysts compared to their unpromoted counterparts (Table S1).

3.2. Molecular structure of surface MO_x sites on TiO_2

Although the TiO_2 support contains ~80% anatase and ~20% rutile, the Raman spectra presented in Fig. 3a are dominated by anatase vibrations (~384, 512, 623 cm^{-1} [68,69] and its weak second-order feature at ~799 cm^{-1} [70]) because of anatase's more efficient light scattering. The *in situ* Raman spectra of the unpromoted supported $WO_3/V_2O_5/TiO_2$ catalysts are shown in Fig. 3b and exhibit Raman bands from surface VO_x (~1030 cm^{-1}) and surface WO_x (~1012 cm^{-1}) sites on the TiO_2 support. The absence of Raman bands from crystalline V_2O_5 (997 cm^{-1}) and WO_3 (805 cm^{-1}) nanoparticles indicates that both of these oxides are fully dispersed on the TiO_2 support [45]. Similarly, the absence of the strong CeO_2 nanoparticle vibrations (464 cm^{-1}) as shown in Fig. 3a indicates that ceria is also well dispersed on the TiO_2 support [27,71]. Furthermore, there is no indication of $Cu_xV_yO_z$ (890 cm^{-1}) [72,73], $CuWO_4$ (910 cm^{-1}) [74], $CeVO_4$ (860 cm^{-1}) [75,76] or $Ce_2(WO_4)_3$ (930 cm^{-1}) [77] nanoparticles being formed in the promoted catalyst. The state of the supported CuO_x phase is not clear from the Raman spectra because of the weak scattering from crystalline CuO/Cu_2O nanoparticles (296 cm^{-1} and 665 cm^{-1}, respectively) [78,79] against the strong TiO_2 background.

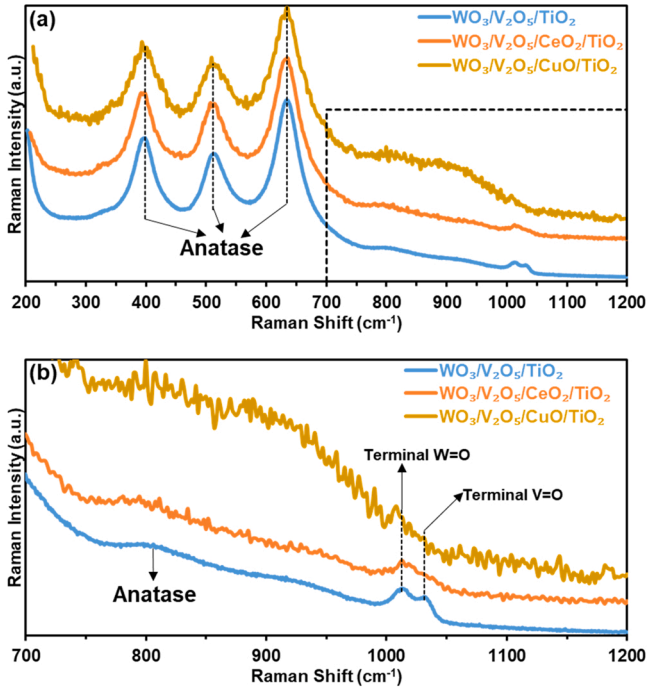

Fig. 3. *In situ* Raman spectra of dehydrated redox promoted supported $WO_3/V_2O_5/TiO_2$ catalysts at 400 °C in flowing 10% O_2/Ar for the spectral regions of (a) 200–1200 cm^{-1} and (b) 700–1200 cm^{-1}.

The molecular structures of the dehydrated supported VO_x WO_x, and SO_x phases on TiO_2 were further investigated with *in situ* IR spectroscopy, and the IR spectra of the catalysts in the overtone region are presented in Fig. 4. The supported V_2O_5/TiO_2 catalyst exhibits the IR V=O vibration at 2039 cm^{-1} (Fig. 4a), with the presence of CeO_x and CuO_x surface sites red shifting the IR V=O vibration to 2036 cm^{-1} (Fig. 4b) and 2021 cm^{-1} (Fig. 4c), respectively, reflecting decreased oligomerization of the surface VO_x sites. Such Ce induced lower VO_x oligomerization has also been demonstrated previously in a sol-gel synthesized 8%CeO_2-92%TiO_2-supported V_2O_5 impregnated catalyst [34]. Impregnation of 5%WO_3 introduces IR W=O vibrations at ~2000–2005 cm^{-1} and induces a blue shift of the IR V=O band in all three catalysts, reflecting increased oligomerization of the surface VO_x sites. This behavior has been shown to be the source of the WO_3 promotional effect in the V_2O_5/TiO_2 SCR system [8]. The introduction of surface sulfate sites weakened the interactions of the surface VO_x and WO_x sites with the Cu promoter and resulted in the V=O band to blue shift to 2046 cm^{-1}, reflecting further oligomerization of the surface VO_x sites. The sulfation of the catalysts shifted the V=O and W=O bands on all catalysts to approximately the same positions, suggesting that the more acidic sulfur displaces surface VO_x and WO_x sites from the Cu promoter. Although the anatase phase signals (384, 512, 623, 796 cm^{-1}) obscure the weak V-O-V (750–830 cm^{-1}) and W-O-W (~780 cm^{-1}) Raman bands [80,81], the shifts in V=O (~2040 cm^{-1}) and W=O (~2000 cm^{-1}) IR overtone bands as discussed above confirm the existence of oligomeric surface structures for the VO_x surface sites. Although the origins of these trends are not presently fully understood, these findings demonstrate that the nature of the surface VO_x sites is strongly affected by the presence of surface oxide promoters.

Impregnation of sulfates into the redox promoted and unpromoted supported $WO_3/V_2O_5/TiO_2$ catalysts introduces new vibrations in the

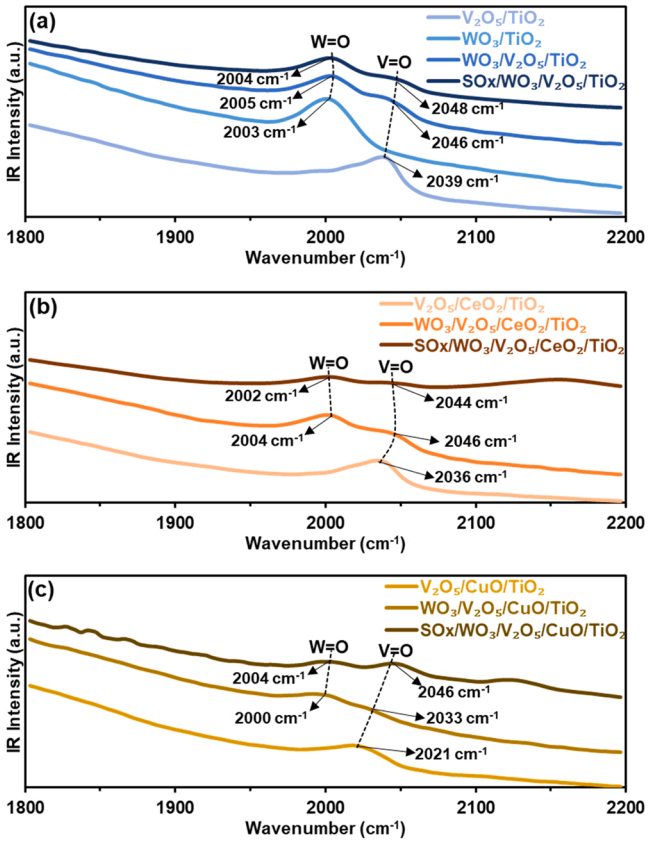

Fig. 4. *In situ* IR spectra of the overtone region for the dehydrated (a) unpromoted catalysts, (b) CeO_x promoted catalysts and (c) CuO_x promoted catalysts (spectra collected at 400 °C in flowing 10% O_2/Ar).

~1300–1380 cm^{-1} region characteristic of surface sulfate vibrations [82–84] as presented in Fig. 5, which confirms that surface sulfates are present in the sulfated catalysts. The vibrations at 1360–1372 cm^{-1} arise from mono-oxo S=O coordinated surface SO_4 sites [82]. The S=O vibrations slightly red shift in the presence of the promoters indicating possible distortion by the redox promoters, with a greater shift observed for the CuO_x promoter than the CeO_x promoter. The IR band at ~1300 cm^{-1} suggests the presence of a second less distorted surface sulfate species for the $SO_x/WO_3/V_2O_5/TiO_2$ catalyst (see Fig. 5) since S-O-M bands vibrate at <1200 cm^{-1} [83,85].

3.3. Surface acidity of supported MO_x/TiO_2 catalysts

3.3.1. Effect of promoters and surface sulfates

The distribution of the Lewis and Brønsted acid sites on the supported MO_x/TiO_2 catalysts was strongly dependent on the specific elements present on the TiO_2 support. The amounts of surface NH_3* and NH_4^+* species on Lewis and Brønsted acid sites, respectively, on the supported MO_x catalysts were quantified by ammonia adsorption coupled with *in situ* IR spectroscopy (Fig. S5). The integrated IR bands of surface NH_3* and NH_4^+* species are presented in Fig. 6. The TiO_2 support possesses only surface Lewis acid sites, and impregnation of the redox CeO_x and CuO_x onto the TiO_2 support decreases the number of surface Lewis acid sites without generating any Brønsted acid sites (Fig. 6a). The lack of any Brønsted acid sites is consistent with the relatively basic character of the surface CeO_x and CuO_x sites [14,64,86]. The decrease in the amount of surface Lewis acid sites reflects the somewhat basic character of the redox promoters relative to the TiO_2 support [64,86] and further indicates that the redox promoters are well dispersed as surface sites that cover the Lewis acid sites of the TiO_2 support. The presence of surface VO_x and WO_x on the TiO_2 support forms Brønsted acid sites and also decreases the number of Lewis acid sites because these surface oxides anchor at the Lewis acid sites of the TiO_2 support. Introduction of surface VO_x (Fig. 6b) and WO_x (Fig. 6c) sites to the CeO_x/TiO_2 support reduces and increases the amount of surface Lewis acid sites, respectively, while introducing surface Brønsted acid sites in both cases. The addition of VO_x and WO_x (Fig. 6c) to the CuO_x/TiO_2 support, however, does not generate surface Brønsted acid sites and modestly affects the amount of surface Lewis acid sites. This demonstrates the basicity of the surface CuO_x sites that neutralize the Brønsted acidity of the surface VO_x and WO_x sites [87]. This, again, can only occur if the supported CuO_x phase is well-dispersed on the TiO_2 support.

Addition of surface sulfates further affects the surface acidity of the supported MO_x catalysts. Addition of surface sulfate to the unpromoted supported $WO_3/V_2O_5/TiO_2$ catalyst increases the amount of surface Brønsted acid sites and slightly decreases the number of surface Lewis acid sites (Fig. 6c and d). When surface sulfate is added to the CeO_x promoted supported $WO_3/V_2O_5/TiO_2$ catalyst, it eliminates the surface Lewis acid sites and significantly increases the amount of surface Brønsted acid sites. This behavior has been previously observed when SO_4 was added in the sol-gel synthesis of $2\%V_2O_5$-$10\%CeO_2$-TiO_2 catalysts [41]. Impregnation of surface sulfate onto the CuO_x promoted

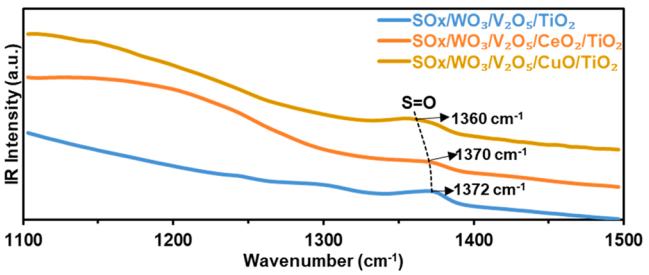

Fig. 5. *In situ* IR spectra of the dehydrated sulfated catalysts.

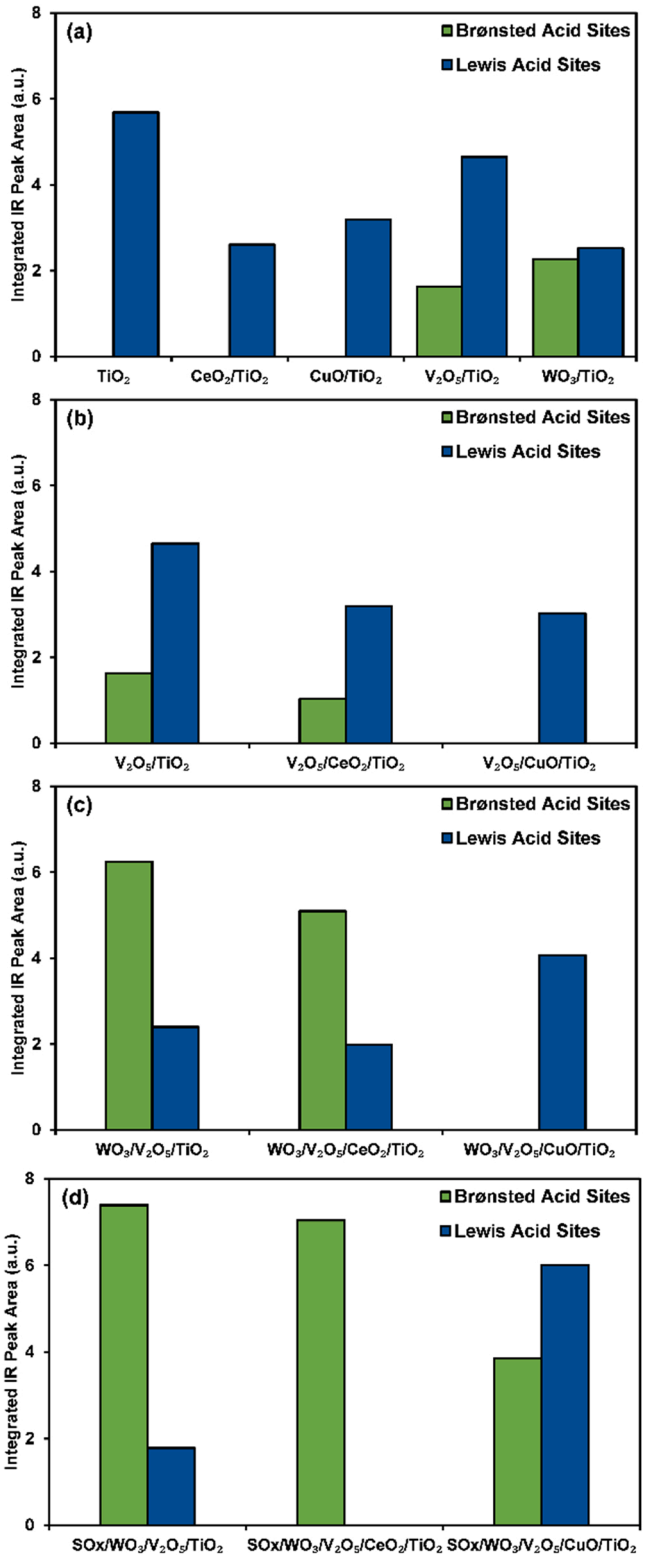

Fig. 6. Effect of surface MO_x on TiO_2 on the amount of surface Lewis and Brønsted acid sites as probed with ammonia adsorption-IR measurements at 110 °C in: (a) supported MO_x/TiO_2 catalysts, (b) supported VO_x impregnated catalysts, (c) supported WO_x impregnated catalysts and (d) supported SO_x impregnated catalysts.

supported $WO_3/V_2O_5/TiO_2$ catalyst increases the amount of surface Lewis acid sites and generates surface Brønsted acid sites, but the amount of surface Brønsted acid sites is much smaller than that of the corresponding CeO_x promoted catalyst, again reflecting the more strongly basic character of the CuO_x surface sites.

3.3.2. *Influence of temperature on surface acid sites of supported MO_x catalysts*

The desorption temperatures of adsorbed NH_4^{+}* (Brønsted) and NH_3 * (Lewis) species on the catalysts are tabulated in Table 1 and reflect the strength of the acid sites (acid strength increases with higher ammonia desorption temperature). The desorption temperature was determined by the disappearance of the surface NH_4^{+}* and NH_3 * signals from the IR spectra. More generally, with the exception of only the sulfated $WO_3/V_2O_5/CuO/TiO_2$ catalyst, the surface NH_3 * species desorb at higher temperatures than from surface NH_4^{+}* species indicating that the surface Lewis acid sites are typically more strongly acidic than the surface Brønsted acid sites. This is further reflected by the decrease in the Brønsted/Lewis acid site number ratio with temperature given in Table S2 and Fig. S6 for the unpromoted and CeO_x promoted catalysts (zero for the CuO_x promoted catalyst due to lack of Brønsted acid sites). This behavior reflects the generally easier desorption of surface NH_4^{+}* species from Brønsted acid sites than surface NH_3 * species from Lewis acid sites. Surface ammonia desorbs at approximately the same temperature from the Brønsted acid sites for sulfate-free CeO_x promoted and unpromoted $WO_3/V_2O_5/TiO_2$ catalysts. The addition of surface sulfate slightly increases the ammonia desorption temperature from Brønsted acid sites for both the CeO_x promoted and unpromoted $WO_3/V_2O_5/TiO_2$ catalysts indicating that surface sulfate introduces stronger acid sites. The sulfate-free CuO_x promoted $WO_3/V_2O_5/TiO_2$ catalyst does not possess any Brønsted acid sites, but weak Brønsted acid sites are introduced by the addition of surface sulfate (desorption temperature of 376 °C). The relatively weak acid sites on the CuO_x promoted catalysts further reflect the basic character of the surface CuO_x sites compared to CeO_x. In general, surface sulfates increase the acid strength of Brønsted acid sites and decrease the acid strength of Lewis acid sites. The findings reveal that the strengths of the surface acid sites are tunable by the promoters and surface sulfates.

3.4. *SCR-TPSR of unpromoted and redox promoted supported MO_x/TiO_2 catalysts*

The supported catalysts were chemically probed by $NO/NH_3/O_2$-TPSR and the resulting spectra are presented in Fig. 7. The unpromoted supported $WO_3/V_2O_5/TiO_2$ catalyst becomes active for SCR at ~180 °C, and reaches ~90% NO conversion at ~370 °C. The conversion of NO slightly decreases at T > 390 °C due to over-oxidation of NH_3 (Fig. 7a).

Table 1
Desorption temperature of adsorbed ammonia species determined with *in situ* IR.

Catalyst	Desorption temperature of NH_4^{+}* from Brønsted acid sites (°C)	Desorption temperature of NH_3 * from Lewis acid sites (°C)
$WO_3/V_2O_5/TiO_2$	424	485
$SO_x/WO_3/V_2O_5/TiO_2$	463	480
$WO_3/V_2O_5/CeO_2/TiO_2$	424	473
$SO_x/WO_3/V_2O_5/CeO_2/TiO_2$	434	–
$WO_3/V_2O_5/CuO/TiO_2$	–	444
$SO_x/WO_3/V_2O_5/CuO/TiO_2$	376	346

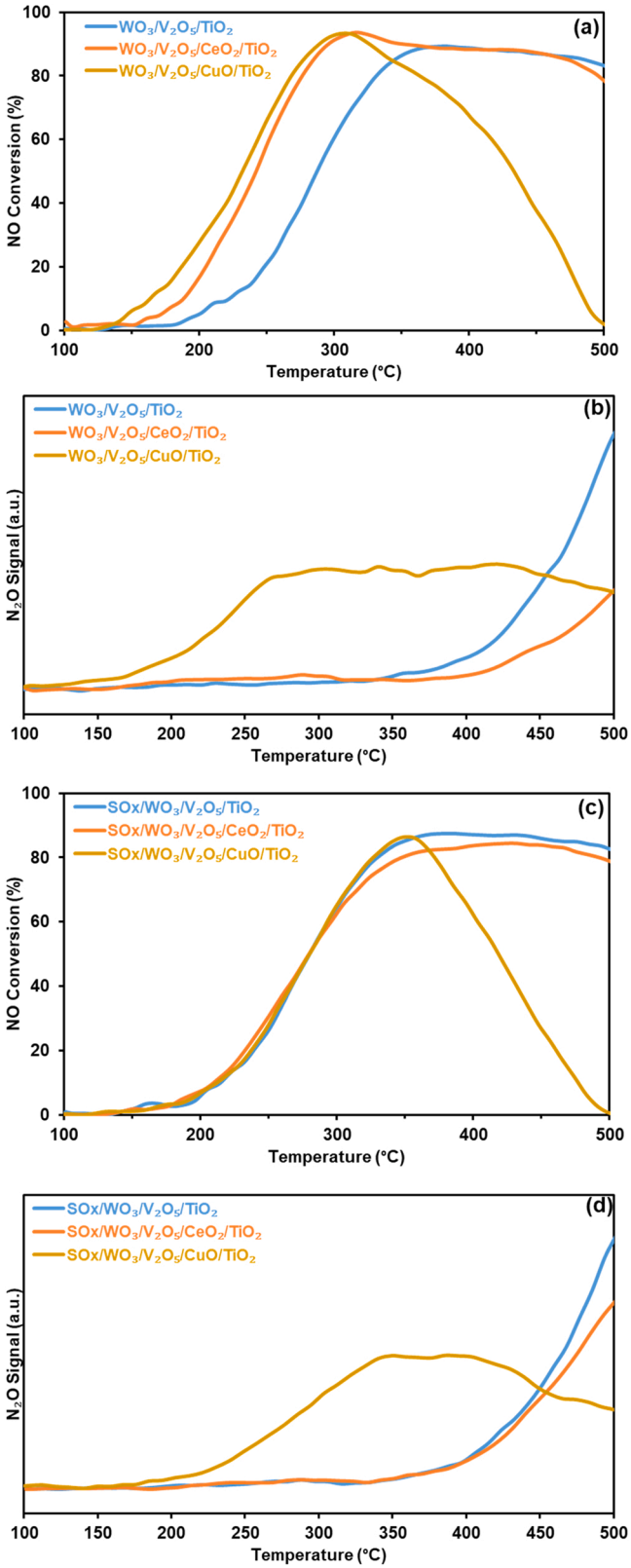

Fig. 7. Comparison of $NO/NH_3/O_2$-TPSR of unpromoted and redox promoted catalysts: (a) NO conversion over the sulfate-free catalysts, (b) N_2O formation over the sulfate-free catalysts, (c) NO conversion over the sulfated catalysts (d) and N_2O formation over the sulfated catalysts.

While both promoted catalysts reach a maximal conversion of ~93%, the CuO_x promoted catalyst requires lower temperatures to reach initial (120 °C vs 150 °C) and complete (305 °C vs 315 °C) NO conversion than the CeO_x promoted catalyst. Of the two, however, only the CeO_x promoted catalyst is capable of maintaining high NO conversion (>85%) over a wide temperature range (280–480 °C), while the over-oxidation of ammonia by the CuO_x promoted catalyst becomes progressively dominant above 315 °C. The unpromoted supported $WO_3/V_2O_5/TiO_2$ catalyst begins producing the N_2O byproduct above ~340 °C while CeO_x promotion suppresses N_2O production and CuO_x promotion enhances N_2O formation (Fig. 7b). The higher NO conversion achieved both at low and high temperatures by supported $WO_3/V_2O_5/CeO_2/TiO_2$ is not due to the redox activity of possibly exposed CeO_x surface sites alone, as evidenced by the low NO conversion of the CeO_2/TiO_2 promoted support (Fig. S7a). Conversely, the CuO_x surface sites seem to be responsible for the supported $WO_3/V_2O_5/CuO/TiO_2$ higher NO conversion at low temperatures, as the CuO/TiO_2 promoted support exhibits similar low temperature conversion performance (Fig. S7a). Furthermore, the decrease in NO conversion at higher temperatures measured for the CuO_x promoted catalysts is already present in the CuO/TiO_2 promoted support, suggesting CuO_x surface sites are responsible for the measured decrease in conversion (Fig. S7a). This decrease is accompanied by high levels of N_2O being formed by the CuO_x promoted surface sites (Fig. S7b) from the over-oxidation of ammonia, as evidenced by the similar levels of generated N_2O when the catalyst was probed with NO-free NH_3/O_2-TPSR (Fig. S8). For both redox-promoted catalysts, the impregnation of the VO_x and WO_x components is vital to reach NO conversion of ~90%, as neither promoted support is capable of reaching such high conversion values (Fig. S7a). These results demonstrate that promotion of the TiO_2 support with CeO_2 has a promotional effect on NH_3 based NO SCR with supported $V_2O_5/WO_3/TiO_2$. This is supported by (a) the initiation of NO conversion at a temperature of ~150 °C compared to ~180 °C for both supported $WO_3/V_2O_5/TiO_2$ and CeO_2/TiO_2 promoted support, and (b) the lower levels of N_2O formed in the CeO_x promoted catalyst compared to its unpromoted counterpart. The enhanced high temperature NO conversion for the CeO_x and CuO_x promoted catalysts could be a result of a promotional effect or simply a product of the combined redox activity of the VO_x and CeO_x/CuO_x surface sites.

The influence of surface sulfates on the activity and selectivity of the unpromoted and redox promoted supported $WO_3/V_2O_5/TiO_2$ catalysts is presented in Fig. 7c and d. The presence of surface SO_x has a negligible effect on the NO conversion and N_2O formation activity (Fig. S9a and b). The addition of surface sulfates to the redox promoted catalysts, however, has a more pronounced effect (Fig. S9c–f). The NO conversion as a function of temperature for both the CeO_x and CuO_x promoted catalysts significantly decreased (Fig. S9c and e) while the N_2O formation activity was inhibited (Fig. S9d and f). The remarkably similar NO conversion activity of all catalysts after sulfation suggests that the interaction of the SO_x surface sites with the redox promoters negated their promotional effect on the NO conversion. Nevertheless, the CeO_x promoted catalyst was capable of maintaining its lower N_2O formation activity after sulfation while exhibiting comparable NO conversion activity to the sulfated unpromoted catalyst.

3.5. Surface structure-activity/selectivity relationships

The catalytic active site for SCR in the supported $V_2O_5/WO_3/TiO_2$ catalyst system is the redox surface VO_x site [5,6]. In the absence of promoters, the surface VO_x sites anchor on the TiO_2 support by forming bridging V-O-Ti bonds. In the presence of the surface CeO_x and CuO_x promoters, with surface coverage of ~0.8 monolayer, the surface VO_x sites also anchor at the surface redox promoters forming bridging V-O-Ce and V-O-Cu bonds in addition to forming V-O-Ti bonds. This is especially true in the Ce promoted catalyst, where the bulk of the sites consumed during VO_x impregnation were the hydroxyls formed during the promotion of TiO_2 by CeO_2. The SCR activity of the catalysts as measured by TPSR did not correlate with the changes in VO_x oligomerization, number or strength of Lewis and/or Brønsted acid sites. Accordingly, it is likely that the enhanced SCR activity of the redox promoted catalysts is at least partially related to a ligand effect through the bridging V-O-Ce/V-O-Cu bonds that enhance SCR redox activity of the surface VO_x sites. Enhanced SCR performance due to Ce-W interactions has been reported before [23,25,29], suggesting that the contribution of W-O-Ce bonds, and possibly W-O-Cu bonds, to the enhanced redox activity reported herein cannot be discounted. The beneficial effect of CeO_x in terms of both SCR activity and selectivity has been previously demonstrated for TiO_2, VO_x/TiO_2 and WO_x/TiO_2 catalytic systems [14,25,34,41]. Both CeO_x [88–92] and CuO_x [35,36,93] surface sites are themselves SCR active as shown on oxide supported systems and herein (Fig. S7). A similar propensity for N_2O generation from ammonia has been shown for CuO/TiO_2 catalysts even without the presence of NO in the gas feed [94]. This behavior could be due to the formation of copper-amine complexes, which tend to decompose into N_2O at the relevant temperatures [95] or direct redox activity by the CuO_x surface sites. The decrease in SCR activity in the redox promoted catalysts after sulaftion could be related to the retardation of the redox properties of the basic surface CeO_x and CuO_x promoters from their recoordination to the acidic surface sulfates rather than the surface VO_x and WO_x sites [96–98].

The series of promoted $WO_3/V_2O_5/TiO_2$ catalysts in this study also allows for the examination of the influence of surface Lewis and Brønsted acid sites on the SCR reaction by supported $WO_3/V_2O_5/TiO_2$ catalysts. The CuO_x promoted $WO_3/V_2O_5/TiO_2$ catalyst only possesses surface Lewis acid sites while the sulfated CeO_x promoted $WO_3/V_2O_5/TiO_2$ catalyst only contains Brønsted acid sites and both catalysts are able to comparably perform the SCR reaction. Since the TPSR data suggests that there are active VO_x sites on both catalysts, this demonstrates that both surface NH_3 * species on Lewis acid sites and surface NH_4^+* species on Brønsted acid sites are able to perform the SCR reaction at comparable reaction rates [99]. The possible differences between the participation of surface NH_3 * species on Lewis acid sites and surface NH_4^+* species on Brønsted acid sites in the SCR reaction are further blurred by the ease of conversion of surface NH_3 * species to surface NH_4^+* species during reaction in the presence of moisture [88,100,101].

4. Conclusions

The results reported herein explore for the first time the fundamental structure-acidity-activity-selectivity relationships of redox promoted (CeO_x and CuO_x), both sulfate-free and sulfated, supported $V_2O_5/WO_3/TiO_2$ catalysts and their effect on the SCR performance. All the supported MO_x phases are present as surface oxide sites on the TiO_2 support and anchor by reacting with surface hydroxyls. The CeO_x and CuO_x redox promoters possess basic character, which decreases the number of surface Lewis acid sites, but their superior redox characteristic accelerates the SCR reaction. The greater redox activity of the CuO_x promoter, however, dominates the SCR reaction and leads to the undesirable over-oxidation of NH_3 (> 305 °C) and formation of the global warming N_2O byproduct (> 120 °C). The redox CeO_x promoter also accelerates the SCR reaction, but does not over-oxidize NH_3 and suppresses formation of the global warming N_2O byproduct (> 400 °C). Sulfation of the unpromoted supported $V_2O_5/WO_3/TiO_2$ SCR catalysts has almost no effect on the SCR activity. Sulfation of the redox promoted supported $V_2O_5/WO_3/TiO_2$ SCR catalysts, however, slows the SCR activity, presumably by bonding to the redox promoters and retarding their redox activity. Although both promoters enhance the catalytic activity, only a small share of VO_x anchor on Cu-(OH)-Cu surface hydroxyls indicating limited direct interaction between CuO_x and VO_x surface sites. This suggests that while both promoters improve the catalytic activity, CuO_x promotion does so by adding redox active sites while CeO_x promotion enhances SCR activity by a ligand effect. Catalysts with either only surface NH_3 * species or only surface NH_4^+* species were found to efficiently

perform the SCR reaction. This demonstrates that both surface NH_3* species on Lewis acid sites and surface NH_4^+* species on Brønsted acid sites are able to perform the SCR reaction, a subject which has been the source of a long-standing debate about the involvement of one surface ammonia species over the other surface ammonia species in the SCR reaction.

CRediT authorship contribution statement

Mingyu Guo: Investigation, Writing – original draft. **Bar Mosevitzky Lis:** Investigation, Writing – original draft, Writing – review & editing, Visualization. **Michael E. Ford:** Supervision. **Israel E. Wachs:** Conceptualization, Supervision, Writing – review & editing, Project administration, Funding acquisition.

Declaration of Competing Interest

The authors declare that they have no known competing financial interests or personal relationships that could have appeared to influence the work reported in this paper.

Acknowledgements

This work was supported as part of Understanding & Control of Acid Gas-Induced Evolution of Materials for Energy (UNCAGE-ME), an Energy Frontier Research Center funded by the U.S. Department of Energy, Office of Science, Basic Energy Sciences under Award # DE-SC0012577. Ms. Mingyu Guo is grateful for the financial support of the scholarship from Tianjin University Graduate School and China Scholarship Council (201906250104).

Appendix A. Supporting information

Supplementary data associated with this article can be found in the online version at doi:10.1016/j.apcatb.2022.121108.

References

[1] R.M. Heck, Catalytic abatement of nitrogen oxides-stationary applications, Catal. Today 53 (1999) 519–523, https://doi.org/10.1016/S0920-5861(99)00139-X.
[2] L. Lietti, I. Nova, G. Ramis, L. Dall'Acqua, G. Busca, E. Giamello, P. Forzatti, F. Bregani, Characterization and reactivity of V2O5-MoO3/TiO2 De-NOx SCR catalysts, J. Catal. 187 (1999) 419–435, https://doi.org/10.1006/jcat.1999.2603.
[3] P. Zhao, M. Guo, Q. Liu, L. Fan, J. Han, C. Liu, N. Ji, C. Song, D. Ma, Z. Li, Novel MnaZrbCrcOx catalysts for low temperature NH3-SCR derived from high H2O content flue gas via natural gas combustion, Chem. Eng. J. 378 (2019), 122100, https://doi.org/10.1016/j.cej.2019.122100.
[4] M. Guo, Q. Liu, P. Zhao, J. Han, X. Li, Y. Ha, Z. Fu, C. Song, N. Ji, C. Liu, D. Ma, Z. Li, Promotional effect of SO2 on Cr2O3 catalysts for the marine NH3-SCR reaction, Chem. Eng. J. 361 (2019) 830–838, https://doi.org/10.1016/j.cej.2018.12.100.
[5] M. Zhu, J.-K. Lai, U. Tumuluri, Z. Wu, I.E. Wachs, Nature of active sites and surface intermediates during SCR of NO with NH3 by supported V2O5–WO3/TiO2 catalysts, J. Am. Chem. Soc. 139 (2017) 15624–15627, https://doi.org/10.1021/jacs.7b09646.
[6] L. Lietti, J.L. Alemany, P. Forzatti, G. Busca, G. Ramis, E. Giamello, F. Bregani, Reactivity of V2O5-WO3/TiO2 catalysts in the selective catalytic reduction of nitric oxide by ammonia, Catal. Today 29 (1996) 143–148, https://doi.org/10.1016/0920-5861(95)00250-2.
[7] Y. He, M.E. Ford, M. Zhu, Q. Liu, Z. Wu, I.E. Wachs, Selective catalytic reduction of NO by NH3 with WO3-TiO2 catalysts: Influence of catalyst synthesis method, Appl. Catal. B Environ. 188 (2016) 123–133, https://doi.org/10.1016/j.apcatb.2016.01.072.
[8] N.R. Jaegers, J. Lai, Y. He, E. Walter, D.A. Dixon, M. Vasiliu, Y. Chen, C. Wang, M. Y. Hu, K.T. Mueller, I.E. Wachs, Y. Wang, J.Z. Hu, Mechanism by which tungsten oxide promotes the activity of supported V2O5/TiO2 catalysts for NOx abatement: structural effects revealed by 51 V MAS NMR spectroscopy, Angew. Chem. Int. Ed. 58 (2019) 12609–12616, https://doi.org/10.1002/anie.201904503.
[9] Y. He, M.E. Ford, M. Zhu, Q. Liu, U. Tumuluri, Z. Wu, I.E. Wachs, Influence of catalyst synthesis method on selective catalytic reduction (SCR) of NO by NH3 with V2O5-WO3/TiO2 catalysts, Appl. Catal. B Environ. 193 (2016) 141–150, https://doi.org/10.1016/j.apcatb.2016.04.022.
[10] M. Zhu, J.-K. Lai, I.E. Wachs, Formation of N2O greenhouse gas during SCR of NO with NH3 by supported vanadium oxide catalysts, Appl. Catal. B Environ. 224 (2018) 836–840, https://doi.org/10.1016/j.apcatb.2017.11.029.
[11] C. Wang, S. Yang, H. Chang, Y. Peng, J. Li, Dispersion of tungsten oxide on SCR performance of V2O5-WO3/TiO2: acidity, surface species and catalytic activity, Chem. Eng. J. 225 (2013) 520–527, https://doi.org/10.1016/j.cej.2013.04.005.
[12] T. Ryu, S.B. Hong, Iron-exchanged UZM-35: an active NH3-SCR catalyst at low temperatures, Appl. Catal. B Environ. 266 (2020), 118622, https://doi.org/10.1016/j.apcatb.2020.118622.
[13] S. Zhan, H. Zhang, Y. Zhang, Q. Shi, Y. Li, X. Li, Efficient NH3-SCR removal of NOx with highly ordered mesoporous WO3(χ)-CeO2 at low temperatures, Appl. Catal. B Environ. 203 (2017) 199–209, https://doi.org/10.1016/j.apcatb.2016.10.010.
[14] T.H. Vuong, J. Radnik, J. Rabeah, U. Bentrup, M. Schneider, H. Atia, U. Armbruster, W. Grünert, A. Brückner, Efficient VOx/Ce1– xTixO2 catalysts for low-temperature NH3-SCR: reaction mechanism and active sites assessed by in situ/operando spectroscopy, ACS Catal. 7 (2017) 1693–1705, https://doi.org/10.1021/acscatal.6b03223.
[15] X. Yao, K. Kang, J. Cao, L. Chen, W. Luo, W. Zhao, J. Rong, Y. Chen, Enhancing the denitration performance and anti-K poisoning ability of CeO2-TiO2/P25 catalyst by H2SO4 pretreatment: Structure-activity relationship and mechanism study, Appl. Catal. B Environ. 269 (2020), 118808, https://doi.org/10.1016/j.apcatb.2020.118808.
[16] T.H. Vuong, J. Radnik, E. Kondratenko, M. Schneider, U. Armbruster, A. Brückner, Structure-reactivity relationships in VOx/CexZr1−xO2 catalysts used for low-temperature NH3-SCR of NO, Appl. Catal. B Environ. 197 (2016) 159–167, https://doi.org/10.1016/j.apcatb.2016.03.063.
[17] Y. Peng, W. Si, X. Li, J. Chen, J. Li, J. Crittenden, J. Hao, Investigation of the poisoning mechanism of lead on the CeO2 - WO3 catalyst for the NH3-SCR reaction via in situ IR and Raman spectroscopy measurement, Environ. Sci. Technol. 50 (2016) 9576–9582, https://doi.org/10.1021/acs.est.6b02307.
[18] M. Koebel, M. Elsener, M. Kleemann, Urea-SCR: a promising technique to reduce NOx emissions from automotive diesel engines, Catal. Today 59 (2000) 335–345, https://doi.org/10.1016/S0920-5861(00)00299-6.
[19] S. Sato, S. Sato, M. Hosoya, Improvement of low-temperature performance of the NOx reduction efficiency on the urea-SCR catalysts, in: Proceedings of the SAE International, 2013. ⟨https://doi.org/10.4271/2013-01-1076⟩.
[20] X. Yuan, H. Liu, Y. Gao, Diesel engine SCR control: current development and future challenges, Emiss. Control Sci. Technol. 1 (2015) 121–133, https://doi.org/10.1007/s40825-015-0013-z.
[21] K. Boriboonsomsin, T. Durbin, G. Scora, K. Johnson, D. Sandez, A. Vu, Y. Jiang, A. Burnette, S. Yoon, J. Collins, Z. Dai, C. Fulper, S. Kishan, M. Sabisch, D. Jackson, Real-world exhaust temperature profiles of on-road heavy-duty diesel vehicles equipped with selective catalytic reduction, Sci. Total Environ. 634 (2018) 909–921, https://doi.org/10.1016/j.scitotenv.2018.03.362.
[22] D. Wang, Y. Peng, Q. Yang, F. Hu, J. Li, J. Crittenden, NH3-SCR performance of WO3 blanketed CeO2 with different morphology: balance of surface reducibility and acidity, Catal. Today 332 (2019) 42–48, https://doi.org/10.1016/j.cattod.2018.07.048.
[23] Y. Peng, K. Li, J. Li, Identification of the active sites on CeO2–WO3 catalysts for SCR of NOx with NH3: an in situ IR and Raman spectroscopy study, Appl. Catal. B Environ. 140–141 (2013) 483–492, https://doi.org/10.1016/j.apcatb.2013.04.043.
[24] Z. Lian, W. Shan, M. Wang, H. He, Q. Feng, The balance of acidity and redox capability over modified CeO2 catalyst for the selective catalytic reduction of NO with NH3, J. Environ. Sci. 79 (2019) 273–279, https://doi.org/10.1016/j.jes.2018.11.018.
[25] K.A. Michalow-Mauke, Y. Lu, K. Kowalski, T. Graule, M. Nachtegaal, O. Kröcher, D. Ferri, Flame-made WO3/CeOx-TiO2 catalysts for selective catalytic reduction of NOx by NH3, ACS Catal. 5 (2015) 5657–5672, https://doi.org/10.1021/acscatal.5b01580.
[26] X. Wu, H. Meng, Y. Du, J. Liu, B. Hou, X. Xie, Insight into Cu2O/CuO collaboration in the selective catalytic reduction of NO with NH3: enhanced activity and synergistic mechanism, J. Catal. 384 (2020) 72–87, https://doi.org/10.1016/j.jcat.2020.01.025.
[27] B.M. Reddy, A. Khan, Y. Yamada, T. Kobayashi, S. Loridant, J.C. Volta, Structural characterization of CeO2-TiO2 and V2O5/CeO2-TiO2 catalysts by Raman and XPS techniques, J. Phys. Chem. B 107 (2003) 5162–5167, https://doi.org/10.1021/jp0344601.
[28] M. Badlani, I.E. Wachs, Methanol: a "smart" chemical probe molecule, Catal. Lett. 75 (2001) 137–149, https://doi.org/10.1023/A:1016715520904.
[29] B. Liu, J. Liu, S. Ma, Z. Zhao, Y. Chen, X.-Q. Gong, W. Song, A. Duan, G. Jiang, Mechanistic study of selective catalytic reduction of NO with NH3 on W-doped CeO2 catalysts: unraveling the catalytic cycle and the role of oxygen vacancy, J. Phys. Chem. C 120 (2016) 2271–2283, https://doi.org/10.1021/acs.jpcc.5b11355.
[30] Y. Peng, J. Li, X. Huang, X. Li, W. Su, X. Sun, D. Wang, J. Hao, Deactivation mechanism of potassium on the V2O5/CeO2 catalysts for SCR reaction: acidity, reducibility and adsorbed-NOx, Environ. Sci. Technol. 48 (2014) 4515–4520, https://doi.org/10.1021/es405602a.
[31] Z. Lian, F. Liu, H. He, Enhanced activity of Ti-modified V2O5/CeO2 catalyst for the selective catalytic reduction of NOx with NH3, Ind. Eng. Chem. Res. 53 (2014) 19506–19511, https://doi.org/10.1021/ie504188s.
[32] F. Lin, Q. Wang, J. Zhang, J. Jin, S. Lu, J. Yan, Mechanism and kinetics study on low-temperature NH3-SCR over manganese-cerium composite oxide catalysts, Ind. Eng. Chem. Res. 58 (2019) 22763–22770, https://doi.org/10.1021/acs.iecr.9b04780.

[33] H. Chang, X. Chen, J. Li, L. Ma, C. Wang, C. Liu, J.W. Schwank, J. Hao, Improvement of activity and SO2 tolerance of Sn-modified MnOx–CeO2 catalysts for NH3-SCR at low temperatures, Environ. Sci. Technol. 47 (2013) 5294–5301, https://doi.org/10.1021/es304732h.
[34] Z. Ma, X. Wu, Y. Feng, Z. Si, D. Weng, L. Shi, Low-temperature SCR activity and SO2 deactivation mechanism of Ce-modified V2O5–WO3/TiO2 catalyst, Prog. Nat. Sci. Mater. Int. 25 (2015) 342–352, https://doi.org/10.1016/j.pnsc.2015.07.002.
[35] G. Xie, Z. Liu, Z. Zhu, Q. Liu, J. Ge, Z. Huang, Simultaneous removal of SO2 and NOx from flue gas using a CuO/Al2O3 catalyst sorbent I. Deactivation of SCR activity by SO2 at low temperatures, J. Catal. 224 (2004) 36–41, https://doi.org/10.1016/j.jcat.2004.02.015.
[36] J.H. Kwak, R. Tonkyn, D. Tran, D. Mei, S.J. Cho, L. Kovarik, J.H. Lee, C.H.F. Peden, J. Szanyi, Size-dependent catalytic performance of CuO on γ-Al2O3: NO reduction versus NH3 oxidation, ACS Catal. 2 (2012) 1432–1440, https://doi.org/10.1021/cs3002463.
[37] C. Chen, W. Jia, S. Liu, Y. Cao, The enhancement of CuO modified V2O5-WO3/TiO2 based SCR catalyst for Hg° oxidation in simulated flue gas, Appl. Surf. Sci. 436 (2018) 1022–1029, https://doi.org/10.1016/j.apsusc.2017.12.123.
[38] H. Wang, B. Wang, Q. Sun, Y. Li, W.Q. Xu, J. Li, New insights into the promotional effects of Cu and Fe over V2O5-WO3/TiO2 NH3-SCR catalysts towards oxidation of Hg0, Catal. Commun. 100 (2017) 169–172, https://doi.org/10.1016/j.catcom.2017.06.036.
[39] H. Kamata, H. Ohara, K. Takahashi, A. Yukimura, Y. Seo, SO2 oxidation over the V2O5/TiO2 SCR catalyst, Catal. Lett. 73 (2001) 79–83, https://doi.org/10.1023/A:1009065030750.
[40] L. Duan, Q. Yu, Q. Zhang, Z. Wang, Y. Pan, T. Larssen, J. Tang, J. Mulder, Acid deposition in Asia: emissions, deposition, and ecosystem effects, Atmos. Environ. 146 (2016) 55–69, https://doi.org/10.1016/j.atmosenv.2016.07.018.
[41] J. Arfaoui, A. Ghorbel, C. Petitto, G. Delahay, Novel V2O5-CeO2-TiO2-SO42− nanostructured aerogel catalyst for the low temperature selective catalytic reduction of NO by NH3 in excess O2, Appl. Catal. B Environ. 224 (2018) 264–275, https://doi.org/10.1016/j.apcatb.2017.10.059.
[42] K. Guo, G. Fan, D. Gu, S. Yu, K. Ma, A. Liu, W. Tan, J. Wang, X. Du, W. Zou, C. Tang, L. Dong, Pore size expansion accelerates ammonium bisulfate decomposition for improved sulfur resistance in low-temperature NH3-SCR, ACS Appl. Mater. Interfaces 11 (2019) 4900–4907, https://doi.org/10.1021/acsami.8b15688.
[43] J.P. Dunn, H.G. Stenger, I.E. Wachs, Oxidation of SO2 over supported metal oxide catalysts, J. Catal. 181 (1999) 233–243, https://doi.org/10.1006/jcat.1998.2305.
[44] I.E. Wachs, C.J. Keturakis, Monolayer systems, in: Compr. Inorg. Chem. II, Elsevier, 2013, pp. 131–151, https://doi.org/10.1016/B978-0-08-097774-4.00717-8.
[45] J.-K. Lai, I.E. Wachs, A perspective on the selective catalytic reduction (SCR) of NO with NH3 by supported V2O5–WO3/TiO2 catalysts, ACS Catal. 8 (2018) 6537–6551, https://doi.org/10.1021/acscatal.8b01357.
[46] H. Zhu, M. Shen, Y. Kong, J. Hong, Y. Hu, T. Liu, L. Dong, Y. Chen, C. Jian, Z. Liu, Characterization of copper oxide supported on ceria-modified anatase, J. Mol. Catal. A Chem. 219 (2004) 155–164, https://doi.org/10.1016/j.molcata.2004.04.032.
[47] B. Xu, L. Dong, Y. Chen, Influence of CuO loading on dispersion and reduction behavior of CuO/TiO2 (anatase) system, J. Chem. Soc. Faraday Trans. 94 (1998) 1905–1909, https://doi.org/10.1039/a801603h.
[48] N. Katada, M. Niwa, Y. Murakami, Acidic Property of Silica Monolayers on Metal Oxides Prepared by CVD Method, in: 1994, 333–338. ⟨https://doi.org/10.1016/S0167-2991(08)61842-X⟩.
[49] S. Djerad, M. Crocoll, S. Kureti, L. Tifouti, W. Weisweiler, Effect of oxygen concentration on the NOx reduction with ammonia over V2O5–WO3/TiO2 catalyst, Catal. Today 113 (2006) 208–214, https://doi.org/10.1016/j.cattod.2005.11.067.
[50] M.V. Mathieu, M. Primet, P. Pichat, Infrared study of the surface of titanium dioxides. II. Acidic and basic properties, J. Phys. Chem. 75 (1971) 1221–1226, https://doi.org/10.1021/j100679a008.